DESY-09-065
HU-EP-09/20
MS-TP-09-06
SFB/CPP-09-41

arXiv:0905.3112v2 [hep-lat] 4 Nov 2009

Phase structure of thermal lattice QCD with $N_f = 2$ twisted mass Wilson fermions

E.-M. Ilgenfritz[1,2], K. Jansen[3], M. P. Lombardo[4], M. Müller-Preussker[1], M. Petschlies[1], O. Philipsen[5], L. Zeidlewicz[5]

[1] *Institut für Physik, Humboldt-Universität zu Berlin, D-12489 Berlin, Germany*
[2] *Institut für Theoretische Physik, Universität Heidelberg, D-69120 Heidelberg, Germany*
[3] *DESY, Zeuthen, D-15738 Zeuthen, Germany*
[4] *Laboratori Nazionali di Frascati, INFN, I-100044 Frascati (RM), Italy*
[5] *Institut für Theoretische Physik, Westfälische Wilhelms-Universität Münster, D-48149 Münster, Germany*

Abstract

We present numerical results for the phase diagram of lattice QCD at finite temperature in the formulation with twisted mass Wilson fermions and a tree-level Symanzik-improved gauge action. Our simulations are performed on lattices with temporal extent $N_\tau = 8$, and lattice coupling β ranging from strong coupling to the scaling domain. Covering a wide range in the space spanned by the lattice coupling β and the hopping and twisted mass parameters κ and μ, respectively, we obtain a comprehensive picture of the rich phase structure of the lattice theory. In particular, we verify the existence of an Aoki phase in the strong coupling region and the realisation of the Sharpe-Singleton scenario at intermediate couplings. In the weak coupling region we identify the phase boundary for the physical finite temperature phase transition/crossover. Its shape in the three-dimensional parameter space is consistent with Creutz's conjecture of a cone-shaped thermal transition surface.

1 Introduction

The quark-hadron transition predicted by Quantum Chromodynamics (QCD) is a central aspect in describing strongly interacting matter at finite temperature T. The early universe has passed through this transition, which is now hoped to be reproduced in ultrarelativistic heavy ion collision experiments. With a transition temperature $T_c \sim 150 - 200\,\mathrm{MeV}$, the relevant energy scale is in the inherently non-perturbative regime of QCD, calling for numerical simulations of lattice QCD. We consider net baryon density zero, for which Monte Carlo methods are directly applicable (cf. [1, 2] for a review). Most previous investigations of lattice thermodynamics have used the Kogut-Susskind (KS) staggered fermion formulation or the Wilson fermion formulation, amended by the improvement programme originally laid out by Symanzik [3, 4, 5, 6]. Both approaches have led to predictions for the nature of the transition, the transition temperature and the equation of state [7, 8, 9, 10, 11, 12]. In particular, based on simulations of a staggered action ref. [10] states that the finite temperature transition in continuum QCD at the physical point is analytic with a transition temperature depending on the observable it is extracted from. Given these results on the one hand and the continuing controversy on the universality of the staggered formulation [13, 14] on the other, a check of these findings with fermions of the Wilson type appears desirable - even though the phase structure of the latter is more complex compared to KS fermions due to explicit chiral symmetry breaking at $\mathcal{O}(a)$.

An economic alternative to the computationally involved Symanzik improvement and/or smearing techniques for the Wilson fermion formulation might be Wilson twisted mass (Wtm) fermions [15, 16]. This formulation allows for automatic $\mathcal{O}(a)-$improvement of physically relevant operators by merely tuning Wilson's hopping parameter κ to its critical value (so called maximal twist, cf. [17] for a detailed review), without computational overhead. This fermion discretisation has been studied extensively at zero temperature by the European Twisted Mass Collaboration (ETMC) [18, 19, 20, 21, 22, 23] providing a growing amount of data relevant for tuning to maximal twist, renormalisation factors and setting the scale [24, 25, 26, 27]. In particular, simulations at pseudoscalar masses $m_{\mathrm{PS}} \approx 300\,\mathrm{MeV}$ are now feasible, and considerable progress in controlling cut-off and finite size effects has been achieved by using lattice chiral perturbation theory [28]. The price to pay for automatic improvement is a more complex phase structure of the lattice model due to the introduction of an additional parameter, the twisted mass μ_0, as well as explicit flavour symmetry breaking by the twisted mass term for $\mu_0 \neq 0$.

The aim of our present study is to investigate the applicability of Wtm fermions for lattice thermodynamics with two degenerate quark flavours. For intermediate quark masses only a smooth crossover is expected in this case, which should turn into either a second or first order phase transition as the chiral limit is approached. The latter situation is, of course, very difficult to establish and currently still under debate, for some of the most recent attempts with opposing conclusions, see [29, 30]. In this work, we restrict ourselves to a study of the phase structure of the Wtm fermion model with a temporal lattice size $N_\tau = 8$. This is a prerequisite to establish whether simulations in the physically interesting regime and using automatic $\mathcal{O}(a)$ improvement are feasible

without running into unphysical phases. The results we present here answer this question in the affirmative.

In Sec. 2 we specify the action and observables used in our simulations. The current knowledge about the phase structure for Wilson type fermions at finite temperature and that of Wtm fermions at zero temperature is summarised in Sec. 3. We present our simulation results in Sec. 4 and discuss them in the light of lattice chiral perturbation theory. Finally, Sec. 5 contains a discussion and our conclusions. Preliminary results of this work have already been reported in [31, 32, 33].

2 Action and observables

Our setup consists of a hypercubic lattice $N_\sigma^3 \times N_\tau$ with periodic boundary conditions for the gauge fields, whereas the fermionic fields are subject to (anti-) periodic boundary conditions in the (time) space direction. We use the tree-level Symanzik improved gauge action given by

$$\mathcal{S}_g[U] = \beta \left[c_0 \sum_P \left(1 - \frac{1}{3}\mathrm{Re}(\mathrm{Tr}[U(P)]) \right) + c_1 \sum_R \left(1 - \frac{1}{3}\mathrm{Re}(\mathrm{Tr}[U(R)]) \right) \right] , \quad (1)$$

where $\beta = 6/g_0^2$ with g_0 the bare gauge coupling and $U(P), U(R)$ denote the path-ordered products of link variables along closed loops of length $4a$ (plaquettes) and $6a$ (rectangles), respectively. The weight coefficients satisfy $c_0 + 8\,c_1 = 1$ (normalisation) and $c_1 = -1/12$ (tree-level improvement condition). This choice of gauge action is motivated by allowing us to exploit ETMC's data for $T = 0$.

The Wilson twisted mass action for the fermion sector in the so-called twisted basis reads

$$\mathcal{S}_F[\psi\,, \bar{\psi}\,, U] = a^4 \sum_x \left[\bar{\psi}(x) \left(D_W + m_0 + i\mu_0 \gamma_5 \tau^3 \right) \psi(x) \right] , \quad (2)$$

with $D_W = \gamma_\mu \frac{1}{2a} \left(\nabla_\mu + \nabla_\mu^* \right) - \frac{ar}{2} \nabla_\mu \nabla_\mu^*$ the Wilson-Dirac operator. This action can be rewritten as

$$\mathcal{S}_F[\Psi\,, \bar{\Psi}\,, U] = a^4 \sum_x \left[\bar{\Psi}(x) \big(\gamma_\mu \frac{1}{2a} \left(\nabla_\mu + \nabla_\mu^* \right) - \frac{ar}{2} \mathrm{e}^{-i\omega\gamma_5\tau^3} \nabla_\mu^* \nabla_\mu + M_0 \big) \Psi(x) \right] \quad (3)$$

in the so-called physical basis $\bar{\Psi}$, Ψ, which is related to the twisted basis $\bar{\psi}$, ψ by the non-anomalous chiral rotation

$$\begin{aligned} \Psi &= \exp\left(i \frac{\omega}{2} \gamma_5 \tau^3 \right) \psi \,, \\ \bar{\Psi} &= \bar{\psi} \exp\left(i \frac{\omega}{2} \gamma_5 \tau^3 \right) \,, \end{aligned} \quad (4)$$

with

$$M_0 = \sqrt{m_0^2 + \mu_0^2}\,, \qquad \tan(\omega) = \mu_0 / m_0 \quad (5)$$

denoting the bare polar quark mass and the bare twist angle, respectively. Finally, introducing Wilson's hopping parameter $\kappa = 1/(2am_0 + 8r)$ and rescaling the fermion fields according to $\psi \to \sqrt{a^3/(2\kappa)}\psi$ leads to the familiar form

$$\begin{aligned}\mathcal{S}_F[\psi\,,\bar{\psi}\,,U] = \sum_x \Big[& \bar{\psi}(x)\left(1 + i2\kappa a\mu_0\gamma_5\tau^3\right)\psi(x) \\ & - \kappa\sum_\mu \bar{\psi}(x)\left((r-\gamma_\mu)U_\mu(x)\psi(x+\hat{\mu}) + (r+\gamma_\mu)U_\mu(x-a\hat{\mu})^\dagger\psi(x-\hat{\mu})\right)\Big]\,.\end{aligned} \tag{6}$$

Because of the spin-flavour structure of the twisted mass term, $ia\mu_0\gamma_5\tau^3$, parity is only a symmetry when combined with a discrete flavour rotation or a sign change $\mu_0 \to -\mu_0$, while flavour symmetry is broken explicitly according to the pattern $SU_V(2) \to U_{(3)}(1)$, where $U_{(3)}(1)$ is the subgroup of flavour rotations generated by τ^3.

For our numerical simulations we use a generalised hybrid Monte-Carlo algorithm with even-odd preconditioning [34], Hasenbusch trick [35, 36] and multiple time scale integration according to the Sexton-Weingarten scheme [37] (cf. [38] for algorithmic benchmarks and [39] for a more recent collection of algorithmic improvements).

In our investigation of the phase structure we measure and analyse the following observables:

1. (averaged) plaquette P

$$P = \frac{1}{6N_\sigma^3 N_\tau}\sum_x\sum_{\mu<\nu}\mathrm{Tr}\left[U_\mu(x)U_\nu(x+\hat{\mu})U_\mu(x+\hat{\nu})^\dagger U_\nu(x)^\dagger\right]\,, \tag{7}$$

2. (real and imaginary part of the) Polyakov loop L

$$L = \frac{1}{3N_\sigma^3}\sum_{\vec{x}}\mathrm{Tr}\left[\prod_{i=0}^{N_\tau-1}U_4(\vec{x},i)\right]\,, \tag{8}$$

3. their susceptibilities according to

$$\chi(\mathcal{O}) = N_\sigma^3\left(\langle\mathcal{O}^2\rangle - \langle\mathcal{O}\rangle^2\right)\,, \tag{9}$$

4. fermionic observables: scalar condensate $\langle\bar{\psi}\psi\rangle$, the order parameter for parity-flavour symmetry breaking $\langle\bar{\psi}i\gamma_5\tau^3\psi\rangle$ and the pion norm

$$|\pi|^2 = \sum_x\langle\bar{\psi}(x)\gamma_5\frac{\tau^+}{2}\psi(x)\bar{\psi}(0)\gamma_5\frac{\tau^-}{2}\psi(0)\rangle\,, \tag{10}$$

   where $\tau^\pm = \tau^1 \pm i\tau^2$.

Discontinuous phase transitions are in principle indicated by any observable, but depending on the particular dynamics one may be more sensitive than the other. In particular, the Polyakov loop is an order parameter for $Z(N)$-breaking and hence susceptible to

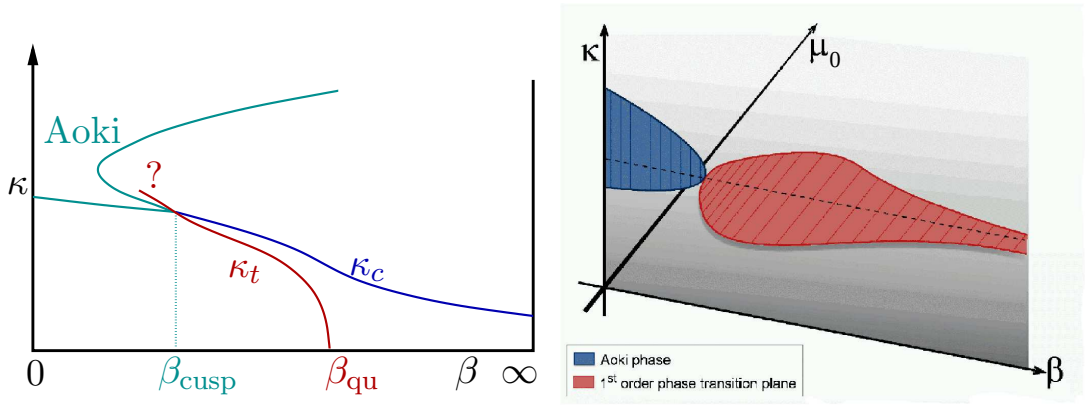

Figure 1: Left: Aoki phase and thermal transition $\kappa_t(\beta)$ for untwisted Wilson fermions. β_{cusp} denotes the tip of the Aoki phase and β_{qu} the critical coupling for the deconfinement transition in the quenched limit. Right: Aoki phase and first order bulk transition for twisted mass Wilson fermions at zero temperature [17].

signals of deconfinement, which get more pronounced the heavier the quark mass. On the other hand, the pion norm and scalar condensate are sensitive to small eigenvalues of the Wtm operator and hence detect signals of chiral symmetry breaking in the light mass regime. The pseudo-scalar condensate is the order parameter for spontaneous parity-flavour symmetry breaking in the plane $\{\mu_0 = 0\}$ of the $(\beta, \kappa, \mu_0)-$parameter space [40, 41, 42].

3 Current knowledge of the phase structure

3.1 Wilson fermions at $T \neq 0$

The phase structure for standard and improved Wilson fermions is determined by two phenomena: spontaneous parity-flavour symmetry breaking and the finite temperature transition. The existence of a phase of spontaneously broken parity-flavour symmetry, commonly called Aoki phase, was introduced theoretically and verified numerically in [40, 41, 43, 44, 45]. Refs. [42, 46, 47, 48] demonstrated that the Aoki phase is located in the strong coupling region and ends in a cusp at a finite β_{cusp}, from which the chiral critical line $\kappa_c(\beta)$ emanates and continues towards the weak coupling limit, cf. Fig. 1 (left). The Aoki phase is repeated for larger values of κ, corresponding to the fermion doubling phenomenon. The value of β_{cusp} depends on the choice of action and the temporal lattice extent. Being a lattice artefact, the Aoki phase does not affect physics in the weak coupling region.

The finite temperature transition or crossover is characterised by a physical transition temperature which depends on the renormalised quark mass, $T_c(m_R)$, and therefore, through m_R, on the bare quark mass. Since $T = 1/(a(\beta)N_\tau)$ on the lattice and the bare quark mass is parametrised in terms of κ, pairs of (m_R, T_c) translate to pairs $(\kappa_t(\beta_c), \beta_c)$

on the lattice describing the phase boundary for finite temperature transitions at fixed N_τ. This line has been mapped out in detail by the CP-PACS [7, 49, 50] and DIK [8, 51, 52] collaborations for the case of an $\mathcal{O}(a)$-Symanzik-improved fermion action on one hand and the standard plaquette or the renormalisation group improved gauge action on the other with the following results:

1. The thermal line for fixed N_τ runs from a finite β_{qu} in the quenched limit ($\kappa_{\mathrm{t}} = 0$), where the transition is of first order, towards the zero temperature chiral critical line $\kappa_{\mathrm{c}}(\beta, T = 0)$ and lower β. This is consistent with the physical expectation that the transition temperature increases with the quark mass.

2. In the vicinity of $\kappa_{\mathrm{c}}(\beta, T = 0)$ and the cusp of the Aoki phase, the thermal line appears to run close and parallel to the critical line; despite large computational efforts a clear separation of the thermal line from the border line of the Aoki phase has not yet been achieved on $N_\tau = 4$ lattices [48] in case of the pure Wilson gauge action.

3.2 Twisted mass fermions at $T = 0$

The zero temperature phase structure of Wilson twisted mass fermions has been investigated in a series of publications by the ETM Collaboration [18, 19, 20, 21, 22, 23]. The parameter space is extended from the $\{\beta, \kappa\}-$plane to the 3d $\{\beta, \kappa, \mu_0\}-$space. Hence, in the strong coupling region an Aoki phase should exist in the $\beta - \kappa-$plane for $0 \leq \beta \leq \beta_{\mathrm{cusp}}$, cf. Fig. 1 (right). Adjacent to it a surface of first order phase transitions extends into the weak coupling region. It is perpendicular to the Aoki phase and includes the chiral transition line at zero twist. This surface is predicted from chiral perturbation theory [53, 54] and has been established in zero temperature simulations [18]. This transition for $\mu_0 > 0$ is also a lattice artefact, correspondingly its width in the μ_0-direction decreases with increasing β and can be made smaller at a fixed value of β by using improved gauge actions [20]. Finite temperatures correspond to finite N_τ on the lattice, which will amount to small shifts of the transition surface compared to $T = 0$.

These unphysical first order transitions and their suppression are a crucial issue for simulations at small quark and corresponding pseudoscalar masses. At maximal twist [25, 26], realised by setting $\kappa = \kappa_{\mathrm{c}}(\beta)$, the width of the surface in μ_0-direction implies a lower bound $\mu_{0\mathrm{c}}(\beta)$ for the twisted mass and hence for the quark mass (cf. Eq. (5)) at fixed β, in order to avoid unphysical phase transitions.

3.3 Twisted mass fermions at $T \neq 0$: Creutz's cone conjecture

In [55, 56] Creutz conjectured a finite temperature phase structure for untwisted and twisted Wilson fermions based on continuum symmetry arguments.

In the continuum theory the twist angle $\tan(\omega) = \mu_0/m_0$ is an irrelevant parameter and the rotation $\exp(i\omega/2\gamma_5\tau^3)$ a mere change of integration variables in the path integral, leaving the path integral measure invariant. Hence, T_c can only be a function of

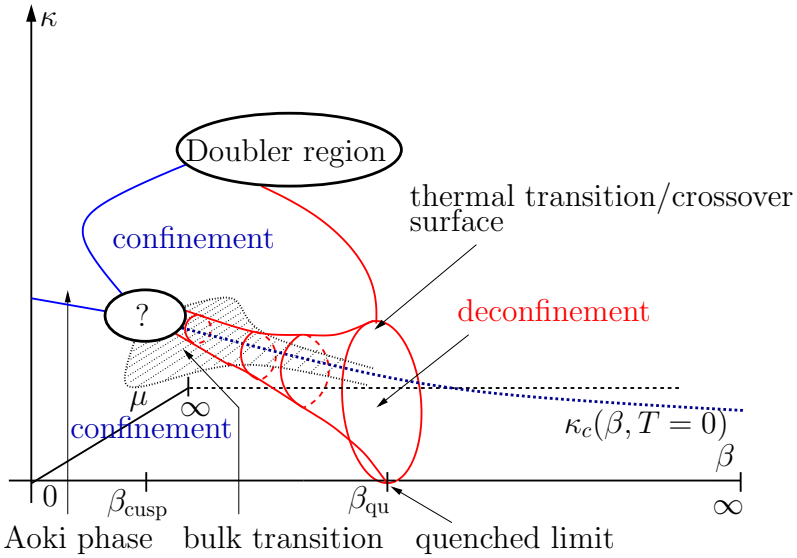

Figure 2: Schematic view of Creutz's cone conjecture, derived from [56].

the renormalised quark mass $M_R = \sqrt{m_R^2 + \mu_R^2}$, i. e. T_c is constant on lines of constant M_R, which correspond to circles. In bare parameter space, because of the renormalisation factors for the masses these curves are ellipses. This picture should translate to the lattice, modified by cut-off effects. For fixed β, the lines of constant M_R are closed curves that become ellipses in the continuum limit. Hence, for fixed N_τ there should be an interval $\beta_{\text{cusp}} \lesssim \beta \lesssim \beta_{\text{qu}}$ where the surface of finite T transitions wraps around the chiral transition line. Since T_c grows with M_R, this surface should have a conical shape opening in the direction of growing β. Fig. 2 gives a schematic summary of the expected phase structure.

While the existence of a finite temperature transition for every value of the twist angle is dictated by the continuum theory, the strength and nature of the transition are subject to discretisation effects and thus generically dependent on the twist angle ω. This will lead to a distortion of the ellipse and conical shape. For sufficiently light quarks, this expectation can be made more quantitative in the framework of lattice chiral perturbation theory. At next-to-leading order (NLO), the expression for the pion mass is [57, 58]

$$m_{\pi^\pm}^2 = M' + \frac{16}{f^2}\left((2L_{68} - L_{45})(M')^2 + M'\hat{a}\cos(\omega)(2W - \tilde{W}) + 2\hat{a}^2\cos^2(\omega)W'\right) \quad (11)$$
$$+\frac{(M')^2}{2\Lambda_\chi^2}\ln\left(\frac{M'}{\Lambda_R}\right) ,$$

where the quark masses are now renormalised ones, $\mu = Z_\mu\mu_0$, $m = Z_m(m_0 - m_c)$. Furthermore, $M' = \sqrt{\hat{\mu}^2 + (\hat{m}')^2}$, $\hat{a} = 2W_0 a$, and $\hat{\mu} = 2B_0 Z_\mu \mu_0$, $\hat{m}' = 2B_0 Z_m(m_0 - m_c)$. The B's, W's, L's can in principle all be fixed by fitting lattice chiral perturbation theory to zero temperature simulation results. Currently, this is not completed yet. Once the NLO formula describes the data sufficiently well, knowledge of one thermal transition point on the cone will suffice to predict the entire distorted ellipse for a given β and pion

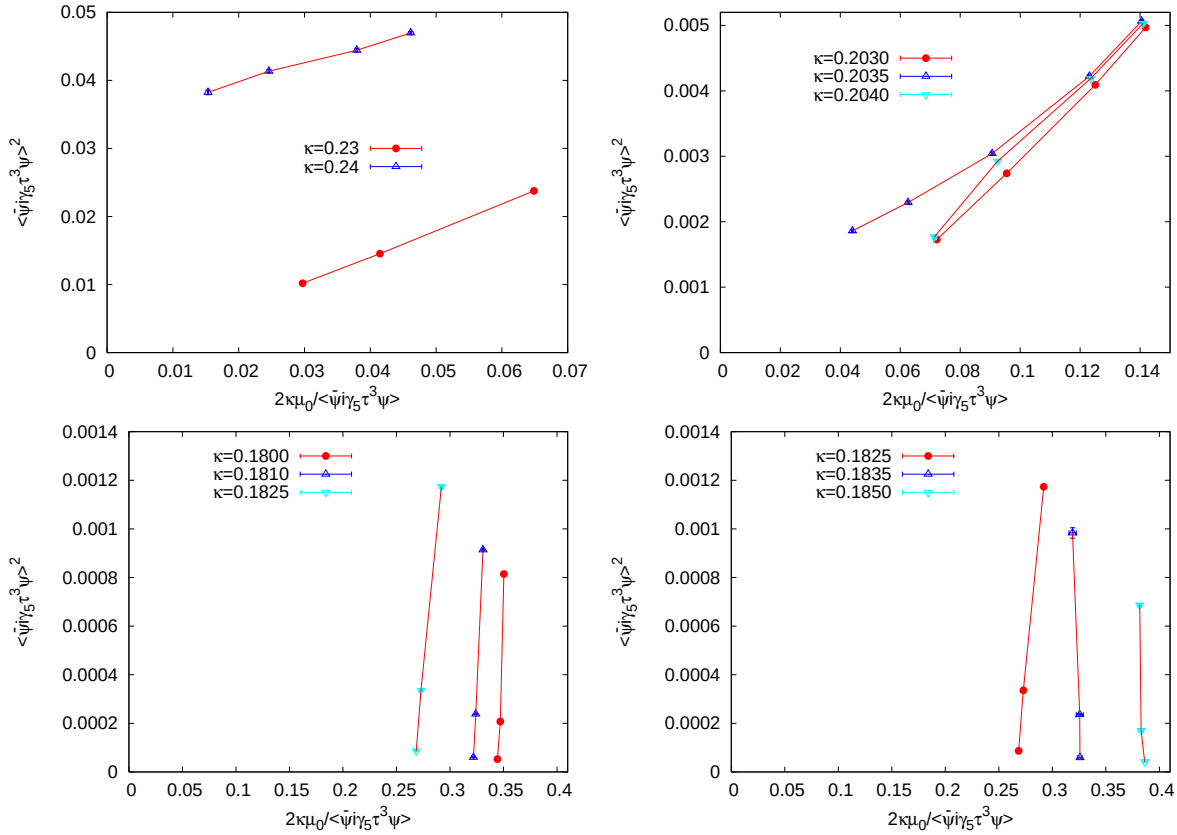

Figure 3: Fisher plots for $\beta = 1.8$ (upper left panel), $\beta = 3.0$ (upper right panel) and $\beta = 3.4$ (lower panels) for $\kappa < \kappa_c \approx 0.1825$ (left) and $\kappa > \kappa_c$ (right).

mass.

4 Simulation results

The goal of our numerical simulations is to establish and locate the different phases discussed in the previous section. The following analysis of our numerical data thus proceeds along the $\beta-$axis from strong coupling ($\beta \lesssim 1.8$) to the scaling region ($\beta \gtrsim 3.8$). The parameter sets for which simulations have been carried out are quoted in Tab. 1 in the Appendix. Throughout this paper we have used lattices with temporal size $N_\tau = 8$ and spatial size $N_\sigma = 16$, except in a few cases where it will be indicated explicitly.

4.1 Strong coupling: the Aoki phase

We checked for the existence of an Aoki phase at $\beta = 1.8, 3.0, 3.4$. For the analysis we consider so-called Fisher plots showing $\langle\bar{\psi}i\gamma_5\tau^3\psi\rangle^2$ as a function of $2\kappa\mu_0/\langle\bar{\psi}i\gamma_5\tau^3\psi\rangle$ (cf. [42] and references therein for a motivation of this approach). One then inspects the behaviour in the limit $2\kappa\mu_0/\langle\bar{\psi}i\gamma_5\tau^3\psi\rangle \to 0$: for $(\beta,\, \kappa)$ points outside the Aoki phase

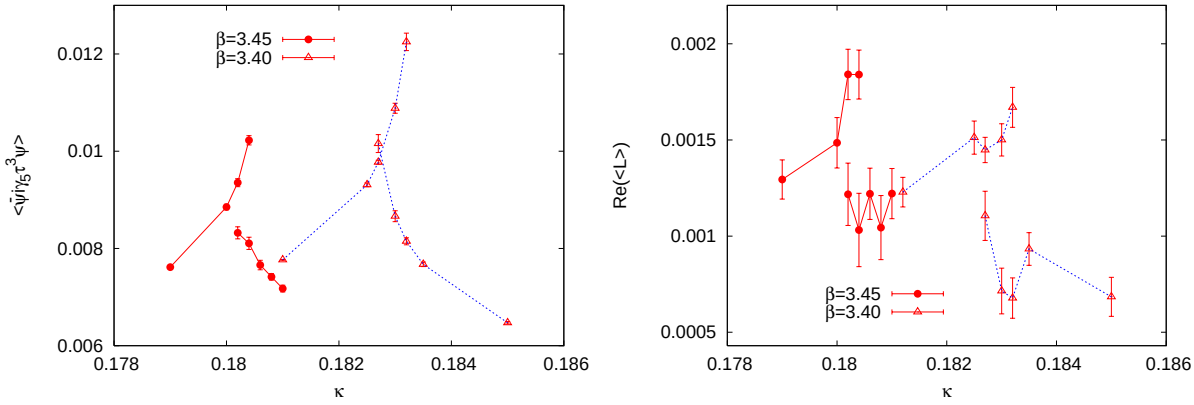

Figure 4: Metastability signals in the order parameter $\langle\bar{\psi}i\gamma_5\tau^3\psi\rangle$ (left) and the Polyakov loop (right) in the neighbourhood of the critical line, $\mu_0 \approx 0.0068$. The lines were added for visual guidance.

the curves will hit the abscissae at a non-vanishing value of $2\kappa\mu_0/\langle\bar{\psi}i\gamma_5\tau^3\psi\rangle$, a point on the phase boundary would lead to a straight line through the origin and a point within the Aoki phase would show a positive intercept with the ordinate axis. Our results are shown in Fig. 3.

The upper left panel shows the situation for the strongest coupling we considered, $\beta = 1.8$. We checked for finite-volume effects on lattices with $N_\sigma = 16$, 24, 32 and found them to be negligible within the statistical uncertainty. From the curves we conclude that the point $(\beta,\ \kappa) = (1.8,\ 0.24)$ lies inside the Aoki phase, whereas $(\beta,\ \kappa) = (1.8,\ 0.23)$ is outside. At $\beta = 3.0$ the upper right panel suggests that the Aoki phase has narrowed to the interval $0.203 < \kappa < 0.204$. The curve for $\kappa = 0.2035$ was measured for $N_\sigma = 16$ only. The point $(\beta,\ \kappa) = (3.0,\ 0.2035)$ appears to be a candidate for spontaneous parity-flavour symmetry breaking.

4.2 Intermediate coupling: the Sharpe-Singleton scenario

The situation changes notably when proceeding to $\beta = 3.4$, as shown in the lower panels of Fig. 3. Neither below nor above $\kappa_c \approx 0.1825$ do we see any indication of spontaneous symmetry breaking. Hence, within our resolution the existence of an Aoki phase is ruled out for $\beta = 3.4$. This assertion is supported by the emergence of another phenomenon. We find clear signals of metastability in all observables when scanning in κ across the region of the chiral critical line, provided μ_0 was chosen small enough. Fig. 4 shows this behaviour for two different observables. We interpret these two-state signals as tied to the surface of first order phase transitions discussed in Sec. 3.2. (Note that in [59] metastability signals were also reported in simulations with pure Wilson fermions at finite temperature and $N_\tau = 6$).

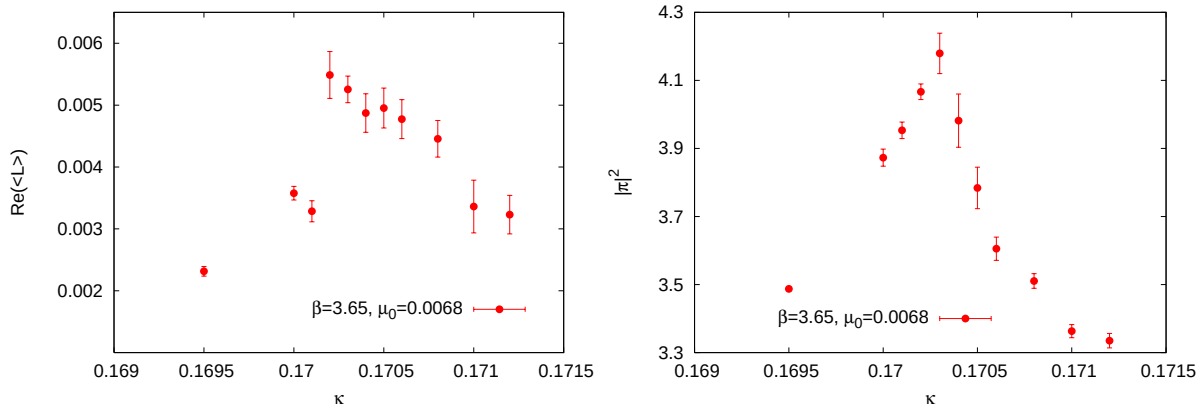

Figure 5: Real part of the Polaykov loop (left) and the pion norm (right) around κ_c at $\beta = 3.65$ and $\mu_0 = 0.0068$.

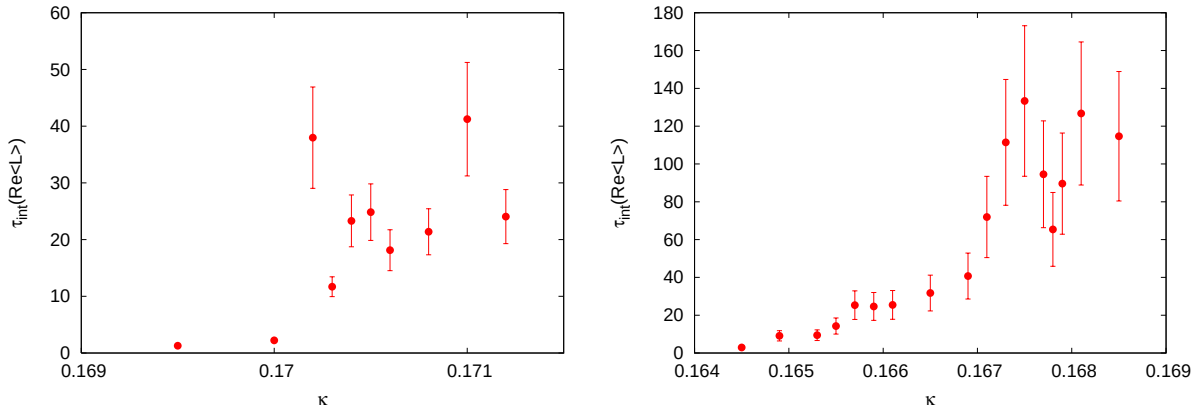

Figure 6: Integrated autocorrelation time for $\mathrm{Re}(L)$ as a function of κ for $\beta = 3.65$, $\mu_0 = 0.0068$ (left) and $\beta = 3.75$, $\mu_0 = 0.0070$ (right).

4.3 Weak coupling: finite temperature transition near κ_c

In this section we discuss our observations of the finite temperature transition, specifically its evolution along the $\beta-$axis. Despite the reasonable statistics of typically $\mathcal{O}(15\mathrm{K})$ trajectories per data point, our results are still noisy and remain somewhat qualitative. This is also due to the fact that we are, most likely, dealing with a very soft crossover rather than a true phase transition.

Let us start by reconsidering the right panel of Fig. 4. The real part of the Polyakov loop rises significantly when κ is increased, indicating the transition to a deconfined regime. Upon crossing κ_c, however, it enters the metastability region discussed in the previous section and then drops again. We interpret the rise and fall of the Polyakov loop along the qualitative expectations from Fig. 2 as an indication for two finite temperature transitions: first a confinement $\rightarrow$ deconfinement transition when approaching κ_c from below, followed by a deconfinement $\rightarrow$ confinement transition at $\kappa > \kappa_c$. This finite temperature transition is masked by the unphysical bulk transition around κ_c if μ_0 is

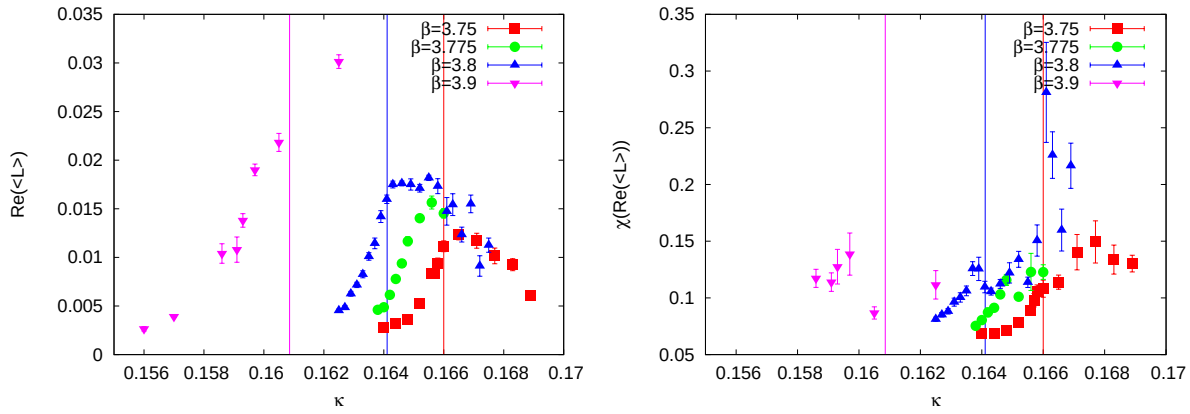

Figure 7: The real part of the Polyakov loop (left) and its susceptibility (right) for $\beta = 3.75, 3.775, 3.8, 3.9$ and $\mu_0 = 0.005$. The vertical lines mark $\kappa_c(T = 0, \beta)$ for $\beta = 3.9, 3.8, 3.75$ from left to right.

chosen too small. However, according to Sec. 3.2 this should be disentangled at larger values of β.

Indeed, choosing $\beta = 3.65$ while keeping μ_0 constant, we observe the behaviour displayed in Fig. 5. The metastabilities are now suppressed and $\langle \mathrm{Re}(L) \rangle$ peaks before gently declining again. Similar signals are obtained from other observables, with a sharper peak in the pion norm marking the chiral transition at κ_c, a remnant from the zero temperature bulk transition.

An inspection of the data points and their statistical uncertainties reveals an asymmetry between $\kappa < \kappa_c$ and $\kappa > \kappa_c$. This is because for $\kappa > \kappa_c$ the spectrum of the twisted mass Dirac operator is shifted in the negative real direction, which implies the occurence of very small eigenvalues and negative quark masses [60]. The results of an autocorrelation analysis are shown in Fig. 6. The integrated autocorrelation time τ_{int} of the Polyakov loop rises notably when passing κ_c, and it continues on a heightened plateau at negative quark masses. Hence, while we believe to have good evidence for its existence, the upper half cone of thermal transitions $\kappa_t > \kappa_c$ is not easily accessible by simulations.

By a further increase of β to $\beta \geq 3.75$ we approach the physically interesting weak bare coupling region. Looking at the left panel of Fig. 7, we once more find the real part of the Polyakov loop displaying a maximum around κ_c, which is consistent with the cone structure. Note also that, in agreement with qualitative expectations, the cone is widening at larger β. It is customary to locate phase transitions more precisely by generalised susceptibilities, which mark the points of maximal fluctuations. These are shown on the right hand side of Fig. 7 for the Polyakov loop. The first transition appears to weaken with decreasing β and turns into a rather flat shoulder at $\beta = 3.75$. Decreasing β implies decreasing T_c, and since T_c is an increasing function of quark mass, the transitions for decreasing β-values belong to a sequence of decreasing mass parameters. Our signals are thus consistent with a weakening of the deconfinement transition when moving away from the quenched regime. The latter was roughly located

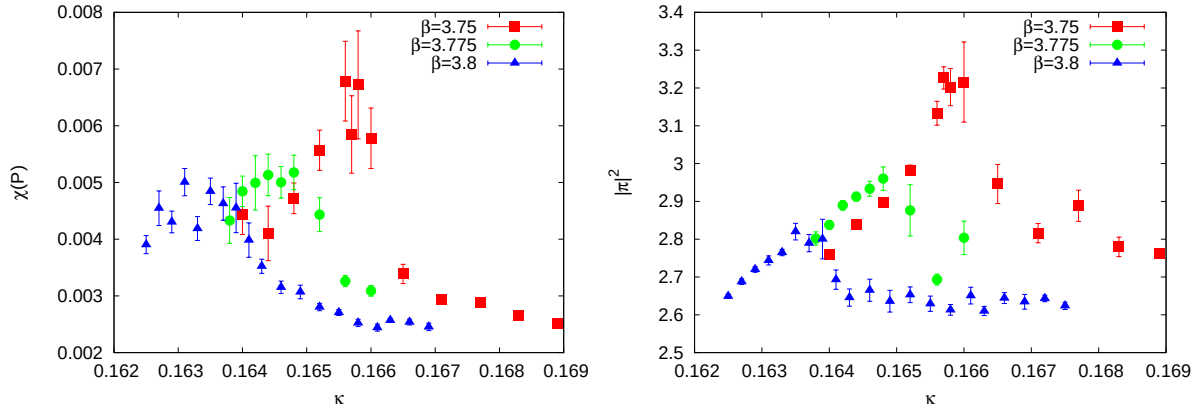

Figure 8: Plaquette susceptibility (left) and pionnorm (right) for $\beta = 3.75, 3.775, 3.8$ and $\mu_0 = 0.005$.

for the tree-level Symanzik improved gauge action by performing a series of $\beta-$scans at very large quark mass and $\mu_0 = 0.005$. As expected [45] the finite temperature transition line bends down from the chiral chritical line towards the $\beta-$axis and hits the latter at a finite value $\beta_{\rm qu} \gtrsim 4.50(5)$ (cf. Table 2).

Fig. 8 shows that the qualitative picture obtained from the Polyakov loop is repeated in the plaquette susceptibility (left) and the pion norm (right). Note that in all cases the location of the first thermal transition is at $\kappa_t < \kappa_{\rm c}$, consistent with the qualitative expectations in Figs. 1, 2. This becomes more obvious in Fig. 9, where we compare in detail the relative position of $\kappa_{\rm c}$ and κ_t for the confinement-deconfinement transition for $\beta = 3.75, 3.8$, as observed in all three observables we consider. Whenever a peak in a susceptibility can be isolated, the value for $\kappa_{\rm t}$ can be consistently determined from any observable by fitting Gaussian curves through the peaks. Our estimated values for the critical couplings are collected in Table 2.

An additional run on a larger lattice does not seem to result in a growth of the susceptibility peaks, as displayed in Fig. 10, a behaviour consistent with a crossover. Our more detailed study at $\beta = 3.75$, which will be reported in Sec. 4.5, will indeed indicate a pion mass over 400 MeV, for which only a smooth crossover behaviour is expected.

The situation changes drastically for $\kappa > \kappa_{\rm c}$: the persistence of the Polyakov loop susceptibility at a high level — a phenomenon we again relate to the peculiar dynamics and its algorithmic problems in this region of quark masses — leaves the localisation of the second transition to be a delicate task. However, we consider the descent of the Polyakov loop as a clear signal for the deconfinement-confinement transition at $\kappa > \kappa_{\rm c}$. We further tested this interpretation by a $\beta-$scan with $\kappa = 0.17$ above κ_c. A signal for a transition was indeed detected and is also given in Table 2.

In contrast to the situation at $\kappa < \kappa_{\rm c}$, these signals are accompanied by a significantly weaker or altogether missing corresponding signal in other observables. This demonstrates the influence of cut-off effects in the simulation of the lattice theory: while the thermal transition in the continuum is manifestly invariant under changes of the

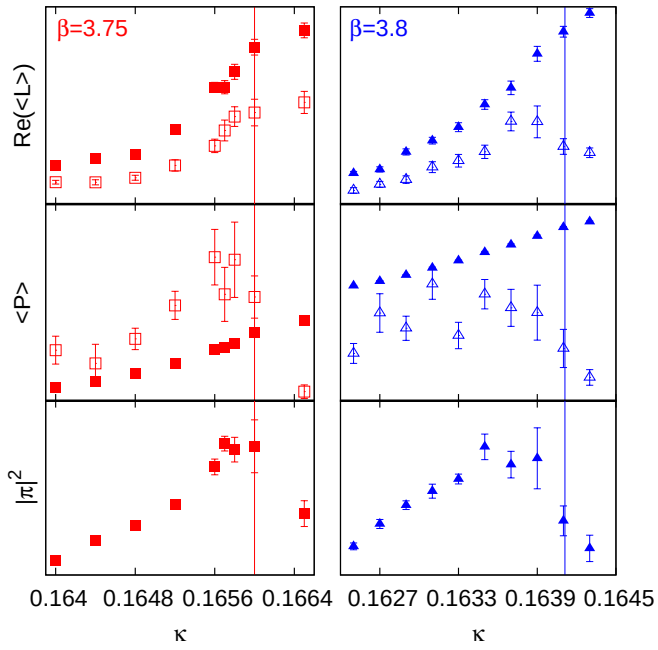

Figure 9: Real part of Polyakov loop (top panel), plaquette (middle panel) and pion norm (bottom) near κ_c (marked by vertical lines). For the first two observables expectation value (filled points) and susceptibility (open) are shown.

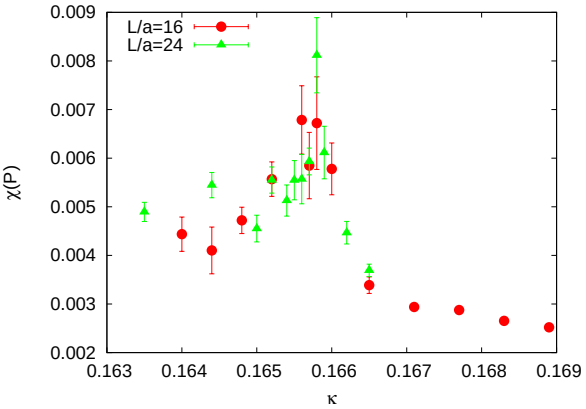

Figure 10: Finite size scaling test for the plaquette susceptibility at $\beta = 3.75$ and $\mu_0 = 0.005$.

twist angle, we find this invariance broken by lattice artefacts such that positive and negative values for the twist angle can result in the two rather distinct signal scenarios we encountered. Let us recall, however, that the physically interesting region is the lower half of the cone with $\kappa \leq \kappa_c$, where the signal for the transition can be located and is consistent among different observables.

4.4 Second branch of finite temperature transitions at large κ

In order to gain a global perspective of the phase structure, we extended our investigation towards $\kappa \gg \kappa_c$, even though this region is not relevant for continuum physics. The results for the Polyakov loop and its susceptibility of several $\kappa-$scans are collected in Fig. 11. There appears to be another line of potential confinement $\rightarrow$ deconfinement transitions moving towards the chiral critical line with increasing β. The existence of such a branch of transitions is consistent with the conjecture in Fig. 2: it matches the line bending upwards from the upper end of the cone at large β towards the first doubler region. In order to give a rough idea of the distance between the two branches we present the data over a large κ-range including also the data near κ_c for $\beta = 3.75$. The distributions of the Polyakov loop in Fig. 12 and especially the pronounced metastability found when simulating on a spatially enlarged lattice with hot and cold starts suggest a

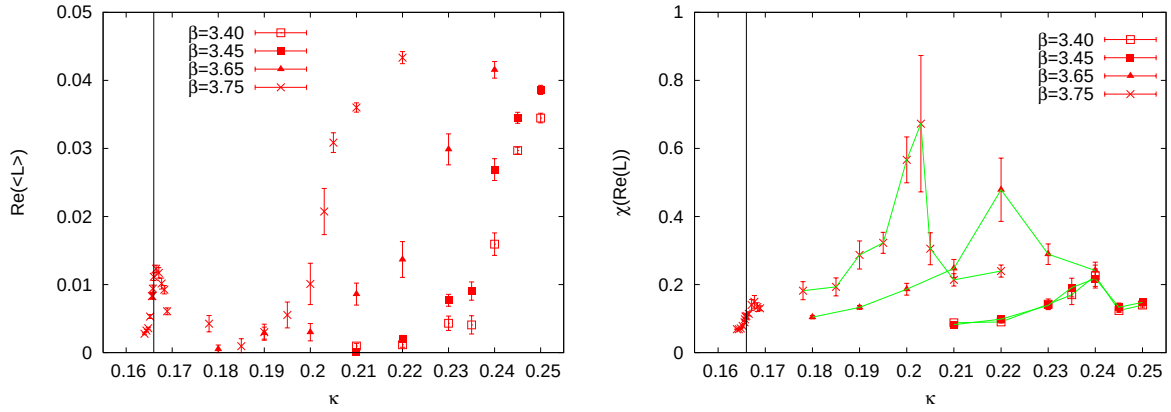

Figure 11: Real part of the Polyakov loop (left) and its susceptibility (right) for $\beta = 3.4, 3.45, 3.65$ with $\mu_0 = 0.0068$ and $\beta = 3.75$ with $\mu_0 = 0.005$. The vertical line marks $\kappa_c(\beta = 3.75)$. Lines on the right are added for visual guidance.

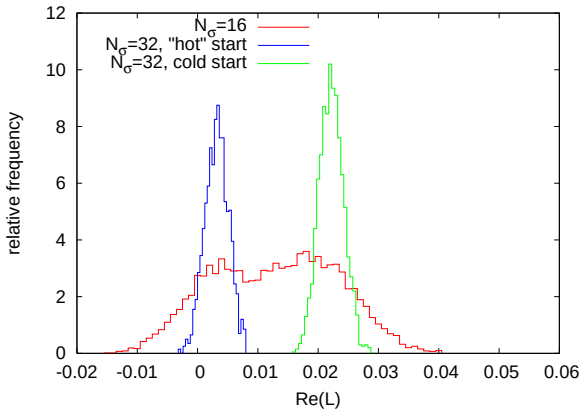

Figure 12: Distributions of Re(L) for $\beta = 3.6, \mu_0 = 0, \kappa = 0.22$.

possible first order nature of the transition in this parameter regime.

4.5 Thermal transition line at fixed β

Having established the overall qualitative phase structure, let us now focus on the shape of the thermal transition surface in a plane of fixed β. To this end we supplement our κ-scan at $\beta = 3.75$, $\mu_0 = 0.005$ from Figs. 7, 8 by additional ones at larger μ_0 values. The qualitative behaviour remains unchanged, but the two thermal transitions should approach each other with increasing μ_0, as expected for a slice of a conical shape. Eventually, for large values of μ_0 one is outside the cone and the transition signal should be lost. This is shown in Fig. 13 (left), where the two transitions can be seen in the rise and fall of the real part of the Polyakov loop. For the largest twisted masses $\mu_0 = 0.025, 0.035$ this behaviour is definitely lost.

In order to locate the transition points more precisely, we have attempted to fit

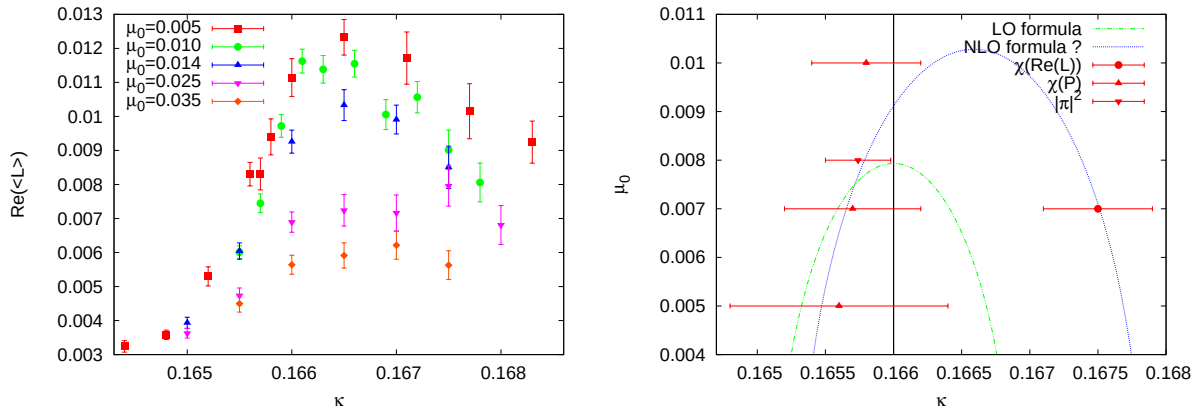

Figure 13: Left: Polyakov loop expectation value for different values of μ_0. For $\mu_0 \geq 0.025$, the transitions are lost. Right: Data points represent the phase boundary at $\beta = 3.75$, estimated from the peaks of susceptibilities. The leading order part of Eq. (11) does not fit the data, the NLO-formula contains undetermined constants that have been estimated by order of magnitude only. The vertical line marks $\kappa_c(\beta = 3.75)$, i.e. maximal twist.

Gaussian curves through the peaks in the susceptibilities, as shown in the examples in Fig. 14. In particular, we may use the clear first transition in Fig. 14 (left) for a rough estimate of the corresponding pion mass. According to Table 2 the thermal transition point κ_t is in this case very close to maximal twist $\kappa_c(\beta = 3.75)$, for which $\mu_0 = 0.005$ corresponds to a pion mass ~ 400 MeV [61]. Since smaller κ_t implies a slightly larger mass, the thermal cone corresponds to a pion $\gtrsim 400$ MeV.

As was discussed before, different observables display signals of different quality, and our data are not precise enough to do an unambiguous determination of both transitions in all observables. Moreover, the underlying physical transition is a broad crossover. For parameter values where entry and exit of the deconfined phase are close, the signals overlap and Gaussian fits do not work reliably, cf. Fig. 14 (right). Nevertheless, in those cases that could be resolved, the peak positions are consistent between all observables, so we have used the observable with the strongest signal in each case. This results in a qualitative picture of the phase boundaries as shown in Fig. 13 (right).

As discussed in Sec. 3.3, in principle the cone of thermal transitions corresponding to a given pion mass at fixed β can be described by lattice chiral perturbation theory, Eq. (11), provided the mass and cut-off effects are sufficiently small. We observe that the leading order formula with only the first term in Eq. (11) is unable to accomodate our data, even if an unknown constant is left open as a fitting parameter. This is not surprising given the large pion mass corresponding to the transition at $\beta = 3.75$. For the NLO curve in Fig. 13 (right) we employed some very rough estimates for the unknown parameters in Eq. (11) to check for consistency with that formula. It would now be interesting to really determine the unknown constants in the full NLO-formula Eq. (11), in order to see whether it correctly describes the data.

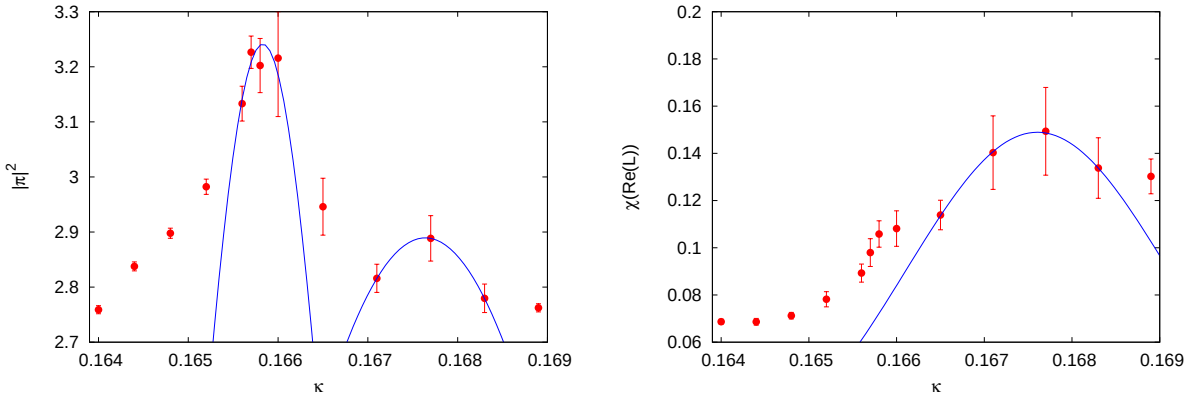

Figure 14: Pion norm (left) and Polyakov loop susceptibility (right) showing two subsequent transitions at $\beta = 3.75, \mu_0 = 0.005$.

5 Discussion and conclusions

We investigated the phase structure of two-flavour Wilson twisted mass fermions at non-zero temperature with special interest in the thermal transition close to the zero temperature chiral critical line. Our estimates for transition points from numerical simulations are summarised in Fig. 15, augmented by data for $\kappa_c(\beta \geq 3.75)$ from the ETM collaboration [24, 61] and the results of a rough tracking of the thermal line towards the quenched limit.

In Fig. 16, we present an expanded view of the scaling region. The values of $r_0 T$ are shown along the upper horizontal axis (cf. reference [21] for the value of r_0/a in the chiral limit). Note that for improved staggered and Wilson fermions, extrapolations of the transition temperature to the chiral limit give $r_0 T_c \sim 0.45$ [8, 62], much smaller than our explored range. This is consistent with our large value of the pion mass and shows that larger $N_t \geq 10$ are required to approach the chiral limit of two flavor QCD.

Using the tree-level Symanzik improved Wilson gauge action, we produced substantial results in support of both the existence of an Aoki phase at strong coupling and the realisation of the Sharpe-Singleton scenario adjacent to the Aoki phase, with a bulk transition surface narrowing towards the weak coupling region. Our results for the thermal transition are consistent with the conical structure proposed in [56].

From our extensive studies exploring a wide range of parameter space we may then conclude that the global phase structure of twisted mass lattice QCD is understood. Moreover, we have shown that for lattices with $N_\tau \geq 8$ this phase structure is beginning to show the features expected in the continuum. In particular, it is then feasible to tune to maximal twist by setting $\kappa = \kappa_c(\beta)$, thus ensuring automatic $O(a)$-improvement, and investigate the thermal transition in the $\{\beta, \mu_0\}$-plane without running into unphysical phases. A recent perturbative study has shown that in this case maximally twisted Wilson fermions show comparable scaling behaviour in the high temperature region as standard staggered fermions [63], while such simulations should not be any more complicated than those with untwisted Wilson fermions. It would thus be interesting to apply

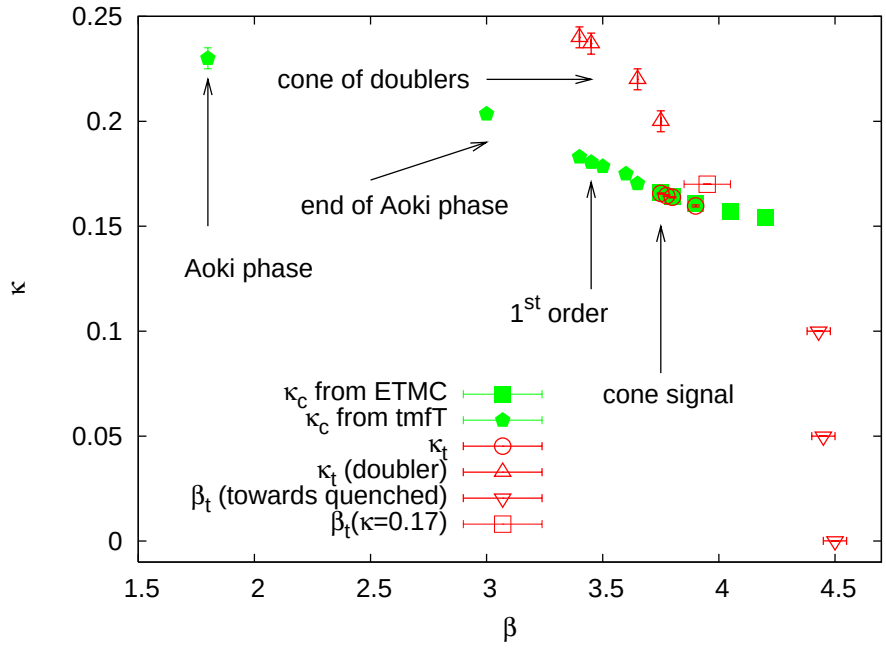

Figure 15: Summary of numerically obtained transition points for $0 \leq \mu_0 \lesssim 0.007$. The data for $\kappa_c(\beta)$, $\beta \geq 3.75$ are taken from [24, 61].

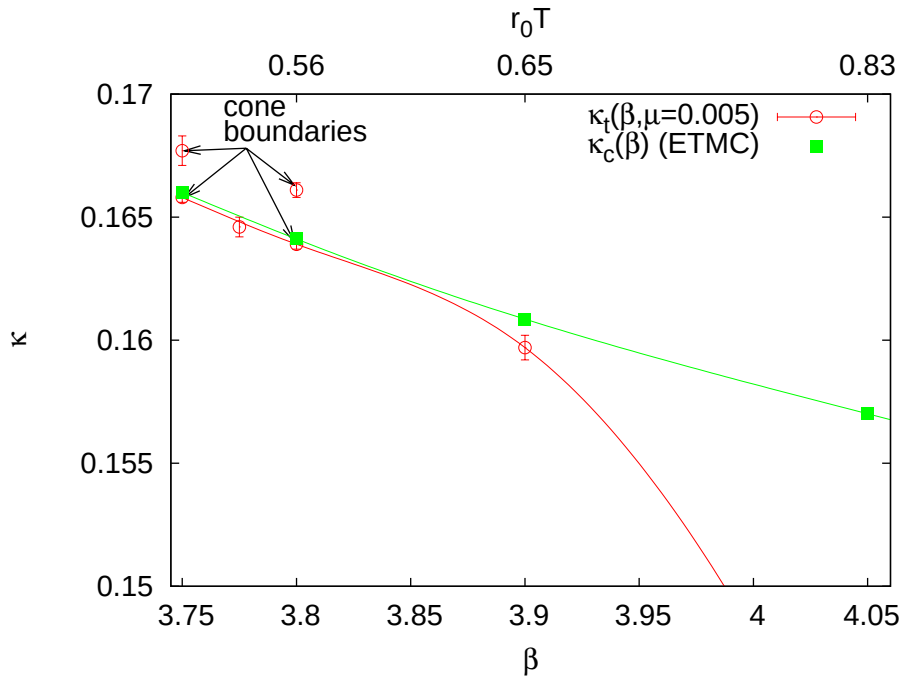

Figure 16: The region $\beta \geq 3.75$. The lines are splines to guide the eye where the quenched and zero coupling limits have been taken into account.

the twisted mass formulation to systematic investigations of QCD thermodynamics.

With results in this direction we hope to come up soon. Employing the twisted mass formulation we would like to add an independent universality check to the resolution of the ongoing controversary concerning the value of the critical temperature(s) and the issue of a possible separation between the deconfining transition and the chiral transition (for a recent paper on this subject see [64] and papers cited therein). We are confident that the automatic $O(a)$ improvement will be technically advantageous for this task. Moreover, the extension to the more realistic case $N_f = 2 + 1 + 1$ seems to be straightforward (see [65]). For studying the thermodynamic state equation, i.e. for computing the pressure or the energy density, as well as the mesonic screening masses as a function of the temperature we do not expect serious complications related to the presence of the twisted mass term. However, in as far the explicit flavor symmetry breaking will affect the thermodynamic behavior remains to be seen.

Acknowledgements: We thank Mike Creutz, Steve Sharpe, André Sternbeck and Carsten Urbach for many useful discussions and again Carsten Urbach for his supply, maintenance and support of the HMC code. We also thank David Schulze for conducting the finite size check on $L = 24$. Most simulations have been done on the apeNEXT computers in Rome and DESY-Zeuthen. This work has been supported in part by the DFG Sonderforschungsbereich/Transregio SFB/TR9. O. P. and L. Z. acknowledge support by the DFG project PH 158/3-1. E.-M. I. was supported by DFG under contract FOR 465 / Mu932/2 (Forschergruppe Gitter-Hadronen-Phänomenologie).

Appendix: Simulation parameters

In Table 1 we give a survey of all parameter sets for the full scan of the phase diagram, ordered according to β. The explored κ range is given as well as the values of the twisted mass parameter μ_0. The last four entries show the β range for scans performed at fixed (κ, μ_0).

In Table 2 we list the locations of the identified thermal transitions κ_t and the observables, from which they were extracted. For the large β values the estimate is based on the distributions of real and imaginary parts of the Polyakov loop. If two values of κ_t are given for the same β and μ_0, this indicates that a sequence of two transitions (interpreted as entrance into and exit out of the cone) could be identified. For $\beta = 3.75$, 3.8 and 3.9 the critical hopping parameter for $T = 0$ (found by the ETM Collaboration [24] at $\mu_0 = 0$) is given for comparison. It should be between the lower and upper κ_t for $\mu_0 \neq 0$.

β	κ	μ_0
1.8	$0.18 \leq \kappa \leq 0.25$	$0.010/(2\kappa)$
1.8	$0.18 \leq \kappa \leq 0.25$	$0.005/(2\kappa)$
1.8	$0.18 \leq \kappa \leq 0.25$	$0.003/(2\kappa)$
3.0	$0.18 \leq \kappa \leq 0.22$	$0.010/(2\kappa)$
3.0	$0.203 \leq \kappa \leq 0.204$	$0.008/(2\kappa)$
3.0	$0.203 \leq \kappa \leq 0.204$	$0.005/(2\kappa)$
3.0	$0.203 \leq \kappa \leq 0.204$	$0.003/(2\kappa)$
3.0	0.2035	$0.0019/(2\kappa)$
3.4	$0.16 \leq \kappa \leq 0.24$	$0.010/(2\kappa)$
3.4	$0.16 \leq \kappa \leq 0.20$	$0.005/(2\kappa)$
3.4	$0.16 \leq \kappa \leq 0.1875$	$0.0025/(2\kappa)$
3.45	$0.179 \leq \kappa \leq 0.1835$	$0.0025/(2\kappa)$
3.65	$0.169 \leq \kappa \leq 0.176$	0.0068
3.75	$0.1640 \leq \kappa \leq 0.1689$	0.005
3.775	$0.1640 \leq \kappa \leq 0.1660$	0.005
3.8	$0.1627 \leq \kappa \leq 0.1675$	0.005
3.9	$0.1550 \leq \kappa \leq 0.1625$	0.005
3.75	$0.1645 \leq \kappa \leq 0.1685$	0.007
3.75	$0.1649 \leq \kappa \leq 0.1677$	0.008
3.75	$0.1655 \leq \kappa \leq 0.1678$	0.010
3.75	$0.1655 \leq \kappa \leq 0.1680$	0.012
3.75	$0.1655 \leq \kappa \leq 0.1670$	0.014
3.75	$0.1650 \leq \kappa \leq 0.1680$	0.025
3.75	$0.1655 \leq \kappa \leq 0.1675$	0.035
3.4	$0.20 \leq \kappa \leq 0.26$	0
3.5	$0.20 \leq \kappa \leq 0.26$	0
3.4	$0.21 \leq \kappa \leq 0.25$	0.0068
3.45	$0.21 \leq \kappa \leq 0.25$	0.0068
3.65	$0.18 \leq \kappa \leq 0.24$	0.0068
3.75	$0.178 \leq \kappa \leq 0.22$	0.005
$3.75 \leq \beta \leq 4.2$	0.17	0.005
$3.7 \leq \beta \leq 5.0$	0.0001	0.005
$3.9 \leq \beta \leq 4.6$	0.05	0.005
$4.0 \leq \beta \leq 4.5$	0.1	0.005

Table 1: Parameter sets for the simulations.

β	κ_{t}	μ_t	$\kappa_{\mathrm{c}}(T=0)$	observable
3.75	0.1656(8)	0.005	0.1660	$\chi(P)$
3.75	0.1677(24)	0.005		$\lvert\pi\rvert^2$
3.75	0.1657(5)	0.007		$\chi(P)$
3.75	0.1675(4)	0.007		$\chi\left(\mathrm{Re}(L)\right)$
3.75	0.16574(24)	0.008		$\lvert\pi\rvert^2$
3.75	0.1658(4)	0.010		$\chi(P)$
3.775	0.1645(1)	0.005		$\chi(P)$
3.8	0.16361(4)	0.005	0.164111	$\lvert\pi\rvert^2$
3.8	0.16621(5)	0.005		$\chi\left(\mathrm{Re}(L)\right)$
3.9	0.1597(3)	0.005	0.160856	$\chi\left(\mathrm{Re}(L)\right)$
3.95(10)	0.17	0.005		$\chi\left(\mathrm{Re}(L)\right)$
4.50(5)	0.0001	0		
4.45(5)	0.05	0		
4.43(5)	0.1	0		

Table 2: Parameter values for identified transition points.

References

[1] O. Philipsen, Eur. Phys. J. Special Topics **152**, 29 (2007), [arXiv:0708.1293].

[2] C. E. DeTar, Proc. Sci. **LATTICE2008**, 001 (2008), [arXiv:0811.2429].

[3] K. Symanzik, Nucl. Phys. **B 226**, 187 (1983).

[4] K. Symanzik, Nucl. Phys. **B 226**, 205 (1983).

[5] M. Lüscher and P. Weisz, Commun. Math. Phys. **97**, 59 (1985).

[6] B. Sheikholeslami and R. Wohlert, Nucl. Phys. **B 259**, 572 (1985).

[7] N. Ukita *et. al.*, Proc. Sci. **LAT2006**, 150 (2006), [hep-lat/0610038].

[8] V. G. Bornyakov *et. al.* (DIK Collaboration), Proc. Sci. **LATTICE2007**, 171 (2007), [arXiv:0711.1427].

[9] Y. Aoki, Z. Fodor, S. D. Katz, and K. K. Szabo, Phys. Lett. **B 643**, 46 (2006), [hep-lat/0609068].

[10] Z. Fodor, Proc. Sci. **LATTICE2007**, 011 (2007), [arXiv:0711.0336].

[11] F. Karsch, Proc. Sci. **CPOD07**, 026 (2007), [arXiv:0711.0656].

[12] F. Karsch, Proc. Sci. **LATTICE2007**, 015 (2007), [arXiv:0711.0661].

[13] M. Creutz, Proc. Sci. **LATTICE2007**, 007 (2007), [arXiv:0708.1295].

[14] A. S. Kronfeld, Proc. Sci. **LATTICE2007**, 016 (2007), [arXiv:0711.0699].

[15] R. Frezzotti, P. A. Grassi, S. Sint, and P. Weisz (Alpha Collaboration), J. High Energy Phys. **08(2001)**, 058 (2001), [hep-lat/0101001].

[16] R. Frezzotti and G. C. Rossi, J. High Energy Phys. **08(2004)**, 007 (2004), [hep-lat/0306014].

[17] A. Shindler, Phys. Rep. **461**, 37 (2008), [arXiv:0707.4093].

[18] F. Farchioni *et. al.*, Eur. Phys. J. **C 39**, 421 (2005), [hep-lat/0406039].

[19] F. Farchioni *et. al.*, Nucl. Phys. Proc. Suppl. **140**, 240 (2005), [hep-lat/0409098].

[20] F. Farchioni *et. al.*, Eur. Phys. J. **C 42**, 73 (2005), [hep-lat/0410031].

[21] F. Farchioni *et. al.*, Proc. Sci. **LAT2005**, 072 (2006), [hep-lat/0509131].

[22] F. Farchioni *et. al.*, Eur. Phys. J. **C 47**, 453 (2006), [hep-lat/0512017].

[23] F. Farchioni *et. al.*, Phys. Lett. **B 624**, 324 (2005), [hep-lat/0506025].

[24] C. Urbach (ETM Collaboration), Proc. Sci. **LATTICE2007**, 022 (2007), [arXiv:0710.1517].

[25] Ph. Boucaud *et. al.* (ETM Collaboration), Phys. Lett. **B 650**, 304 (2007), [hep-lat/0701012].

[26] Ph. Boucaud *et. al.* (ETM Collaboration), Comput. Phys. Commun. **179**, 695 (2008), [arXiv:0803.0224].

[27] P. Dimopoulos *et. al.*, Proc. Sci. **LATTICE2007**, 241 (2007), [arXiv:0710.0975].

[28] P. Dimopoulos *et. al.* (ETM Collaboration), Proc. Sci. **LATTICE2008**, 103 (2008), arXiv:0810.2873.

[29] J. B. Kogut and D. K. Sinclair, Phys. Rev. **D 73**, 074512 (2006), [hep-lat/0603021].

[30] C. Bonati, G. Cossu, A. D'Alessandro, M. D'Elia, and A. Di Giacomo, Proc. Sci. **LATTICE2008**, 252 (2008), [arXiv:0901.4429].

[31] E.-M. Ilgenfritz *et. al.*, Proc. Sci. **LAT2006**, 140 (2006), [hep-lat/0610112].

[32] E.-M. Ilgenfritz *et. al.*, Proc. Sci. **LATTICE2007**, 238 (2007), [arXiv:0710.0569].

[33] E.-M. Ilgenfritz *et. al.*, Proc. Sci. **LATTICE2008**, 206 (2008), [arXiv:0809.5228].

[34] T. A. DeGrand, Comput. Phys. Commun. **52**, 161 (1988).

[35] M. Hasenbusch, Phys. Lett. **B 519**, 177 (2001), [hep-lat/0107019].

[36] M. Hasenbusch, Nucl. Phys. Proc. Suppl. **129**, 27 (2004), [hep-lat/0310029].

[37] D. H. Weingarten and J. C. Sexton, Nucl. Phys. Proc. Suppl. **26**, 613 (1992).

[38] C. Urbach, K. Jansen, A. Shindler, and U. Wenger, Comput. Phys. Commun. **174**, 87 (2006), [hep-lat/0506011].

[39] K. Jansen and C. Urbach, arXiv:0905.3331.

[40] S. Aoki, Phys. Rev. **D 30**, 2653 (1984).

[41] S. Aoki, Nucl. Phys. Proc. Suppl. **60A**, 206 (1998), [hep-lat/9707020].

[42] E.-M. Ilgenfritz, W. Kerler, M. Müller-Preussker, A. Sternbeck, and H. Stüben, Phys. Rev. **D 69**, 074511 (2004), [hep-lat/0309057].

[43] S. Aoki, Phys. Lett. **B 190**, 140 (1987).

[44] S. Aoki, Nucl. Phys. **B 314**, 79 (1989).

[45] S. Aoki, A. Ukawa, and T. Umemura, Phys. Rev. Lett. **76**, 873 (1996), [hep-lat/9508008].

[46] K. M. Bitar, Phys. Rev. **D 56**, 2736 (1997), [hep-lat/9602027].

[47] A. Sternbeck, E.-M. Ilgenfritz, W. Kerler, M. Müller-Preussker, and H. Stüben, Nucl. Phys. Proc. Suppl. **129**, 898 (2004), [hep-lat/0309059].

[48] E.-M. Ilgenfritz, W. Kerler, M. Müller-Preussker, A. Sternbeck, and H. Stüben, hep-lat/0511059.

[49] A. Ali Khan *et. al.* (CP-PACS Collaboration), Phys. Rev. **D 63**, 034502 (2001), [hep-lat/0008011].

[50] A. Ali Khan *et. al.* (CP-PACS Collaboration), Phys. Rev. **D 64**, 074510 (2001), [hep-lat/0103028].

[51] V. G. Bornyakov *et. al.* (DIK Collaboration), Phys. Rev. **D 71**, 114504 (2005), [hep-lat/0401014].

[52] V. G. Bornyakov *et. al.*, Proc. Sci. **LAT2005**, 157 (2006), [hep-lat/0509122].

[53] S. R. Sharpe and R. L. Singleton Jr., Phys. Rev. **D 58**i, 074501 (1998), [hep-lat/9804028].

[54] G. Münster, J. High Energy Phys. **09(2004)**, 035 (2004), [hep-lat/0407006].

[55] M. Creutz, hep-lat/9608024.

[56] M. Creutz, Phys. Rev. **D 76**, 054501 (2007), [arXiv:0706.1207].

[57] S. R. Sharpe and J. M. S. Wu, Phys. Rev. **D 71**, 074501 (2005), [hep-lat/0411021].

[58] S. R. Sharpe, hep-lat/0607016.

[59] T. Blum *et. al.*, Phys. Rev. **D 50**, 3377 (1994), [hep-lat/9404006].

[60] K. Jansen, A. Shindler, C. Urbach, and I. Wetzorke (XLF Collaboration), Phys. Lett. **B 586**, 432 (2004), [hep-lat/0312013].

[61] Carsten Urbach (ETM Collaboration) (private communication).

[62] M. Cheng *et. al.*, Phys. Rev. **D 74**, 054507 (2006), [hep-lat/0608013].

[63] O. Philipsen and L. Zeidlewicz, arXiv:0812.1177.

[64] V.G. Bornyakov *et al.*, arXiv:0910.2392.

[65] R. Baron *et al.* (ETM Collaboration), Proc. Sci. **LATTICE2008**, 094 (2008), [arXiv:0810.3807].